PERGAMON

Engineering Fracture Mechanics 69 (2002) 687–699

Engineering Fracture Mechanics

www.elsevier.com/locate/engfracmech

Experimental and numerical analysis of delamination growth in double cantilever laminated beams

Valeria La Saponara [a], Hanifah Muliana [b], Rami Haj-Ali [b,*], George A. Kardomateas [a]

[a] *School of Aerospace Engineering, Georgia Institute of Technology, Atlanta, GA 30332, USA*
[b] *School of Civil and Environmental Engineering, Georgia Institute of Technology, Atlanta, GA 30332, USA*

Received 6 March 2001; received in revised form 30 July 2001; accepted 3 August 2001

Abstract

Delamination crack growth in laminated composites is investigated using experiments and finite element (FE) models. Tests are performed on cross-ply graphite/epoxy specimens under static conditions. The load–displacement response is monitored in the tested coupons along with crack length. The FE models employ a cohesive layer that is used to simulate the debonding and crack propagation. The cohesive parameters are calibrated from the experimental load–displacement curves. Crack growth and strain measurements are compared with those from the FE models. The predicted results from the FE models are in good agreement with the test results. The same modeling approach is also used to simulate crack propagation in the transverse direction of a notched laminate. The proposed FE analysis with cohesive layers can simplify fracture toughness assessment in multilayered specimens.

Keywords: Graphite/epoxy; Experiment; Composite; Finite element; Cross-ply; Crack; Double cantilever beam; Cohesive; Growth; Laminate

1. Introduction

Delamination is a common type of failure mode in layered composites without through-the-thickness reinforcement. Delaminations are created when two layers debond from each other. The initiation of delamination growth is usually determined by examining Mode I and Mode II fracture toughnesses, that are generally calculated from unidirectional composites. Measuring fracture toughness in a multidirectional composite can be difficult because the crack propagates in a non-self-similar manner, and a mixed-mode loading occurs as soon as the crack initiates. Predicting crack propagation in multidirectional composites can have great impact on the analysis and design of composite materials.

* Corresponding author. Tel.: +1-404-894-4716; fax: +1-404-894-0211.
E-mail address: rami.haj-ali@ce.gatech.edu (R. Haj-Ali).

0013-7944/02/$ - see front matter
PII: S0013-7944(01)00106-0

Many surveys of analytical methods used in solving the interface crack problems exist, e.g. Refs. [1,2]. Two main approaches have been proposed for interface crack problems: (1) the open crack approach, which is based on the work of Williams [3], England [4] and Erdogan [5]; (2) the closed crack approach, introduced by Comninou [6,7] and extended by Gautesen and Dundurs [8,9]. The first approach considers the interface crack as completely open. The solution for the stress includes an oscillatory behavior at the crack tip. This is not physically possible since it would lead to overlapping and wrinkling of the crack faces. Assumptions on the material properties are made to avoid the oscillatory behavior [10,11]. The closed crack approach considers the interface crack open except at the crack tips, where frictionless contact occurs. The length of the contact areas is part of the solution, and no stress oscillation is obtained.

Finite element (FE) models have been utilized in the past to study the stress distribution and the strain energy release rate in cracked composite laminates subject to Mode I, Mode II, and mixed-mode loadings. Van der Zande and Grootenboer [12] compare their model of an interface crack in an isotropic bi-material with Comninou's results [6,7]. They model contact zones at the crack tips with special contact elements, which do not permit wrinkling of the two faces and transmit the compressive stresses in the contact zone of the crack. These authors also use a displacement hybrid model to calculate the elastic stress intensity factors. Hwu et al. [13] use a FE model for delamination analysis of glass/epoxy multidirectional specimens, with lay-ups $[0_n/\pm\theta_n/0_n]$, $\theta = 0°$, 15°, 30°, 45°, and n varying between 3 and 6. Their results compare very well with the experiments in predicting first interface debonding in non-pre-cracked specimens and for the onset of the delamination in pre-cracked specimens. Dakshina Moorthy and Reddy [14] compared four methods for calculating the interlaminar stress and energy release rate: layerwise theory, virtual crack closure, crack closure, and potential energy change. These quantities are calculated in bending problems: simply supported cross-ply laminate under sinusoidal loads, $[\pm 45]_s$ laminate with two free edges and two simply supported edges and cross-ply, double cantilever beam (DCB) laminate. Contact surfaces are assumed on each side of the crack. A no-slip adhesive contact condition is enforced by the penalty method.

Delamination problems in pre-cracked composite laminates have been extensively analyzed. Different methods can be used to calculate strain energy release rate and mode mixity. The Rayleigh–Ritz method is used with classical plate theory by Davidson and Schapery [15]. An analytical crack tip element based on classical plate theory was introduced by Davidson et al. [16,17]. The virtual crack closure technique was used by Davidson [18] and Polaha et al. [19]. Experimental results are also reported for DCB, end-notched flexure and single-leg bending tests in Ref. [19].

This study deals with delamination in layered cross-ply laminates, and cracking in notched laminates. FE models with cohesive layers are used to simulate the debonding. The crack propagation results are compared with tests of pre-cracked DCBs under static loading. The method is also tested for in-plane transverse crack configuration, in $[90]_{20}$ notched-edge laminates under tensile axial loading.

Next, the experimental testing configurations and results are described, followed by the FE models. Finally, discussion and conclusions are presented.

2. Experimental set-up and testing procedure

The specimens in this study are manufactured by hand lay-up and cured in an autoclave. The pre-preg material used was TOHO UT500 graphite/epoxy. The measured effective material properties for a unidirectional lamina are: $E_{11} = 124$ GPa; $E_{22} = 9.60$ GPa; $v_{12} = 0.344$; $G_{12} = 5.75$ GPa.

Two types of specimens are prepared: (a) cross-ply specimens, having lay-up $[0/90]_{10}$, with a 46 mm delamination starter, and average dimensions of 25.4 mm × 137 mm × 2.55 mm, as shown in Fig. 1; (b) transversely reinforced specimens, with $[90]_{20}$ lay-up and two edge notches in their mid-section. Fig. 2 shows the notched laminate with tabs. These are bonded with epoxy to ensure proper gripping during the tensile test. The dimensions of the second group of specimens are: 25.4 mm × 135 mm × 2.62 mm in un-notched

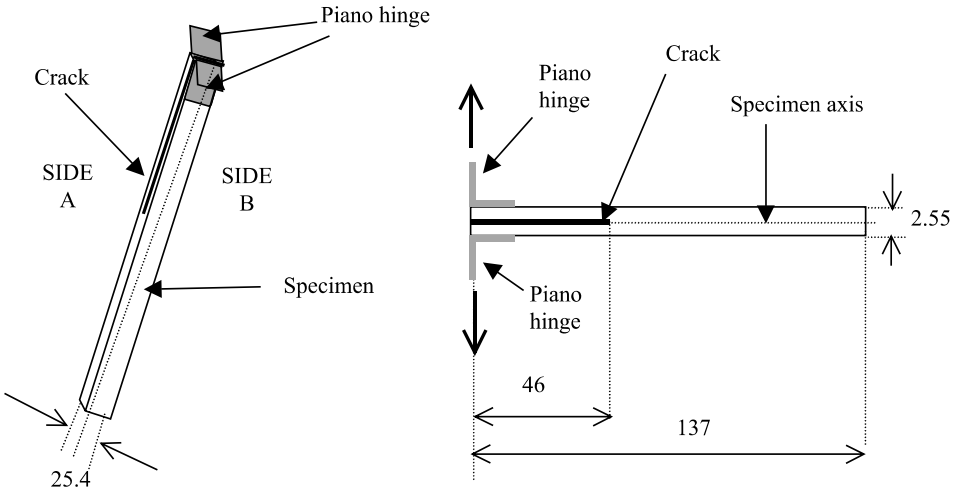

Fig. 1. 3D and side views of a cross-ply specimen for DCB tests (dimensions are in mm and not to scale).

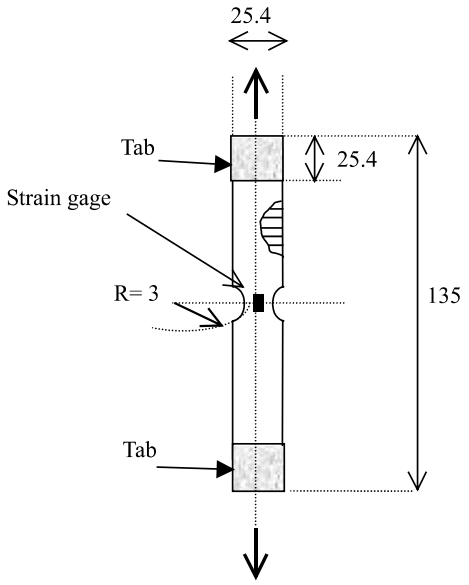

Fig. 2. Notched laminated $[90]_{20}$ under uniaxial tension (dimensions are in mm and not to scale).

sections, and 19.2 mm × 135 mm × 2.62 mm in notched sections. In the delamination tests, piano hinges are bonded to the specimen by either a double-sided adhesive (with designation AF163 2K, produced by 3M) or epoxy glue. The delamination starter in these specimens consisted of a Teflon thin sheet inserted during lay-up between the 10th and the 11th ply, at the mid-plane of the beam.

Two experimental procedures are performed: (a) DCB tests on delaminated cross-ply specimens; (b) axial tensile tests of notched laminated specimens.

The tests were performed using an Instron 8501 hydraulic testing machine with a 100 KN load cell. The displacement of the moving lower cross-head (the actuator) with respect to the upper cross-head (fixed) is

recorded. A Questar QM-1 microscope and a remote video measurement system are used to follow crack propagation. The edges of the DCB specimens are sprayed with white paint and marks are drawn on each edge, 1 mm apart from each other. In the notched laminated specimens, marks are drawn between the two notches. A displacement rate of 0.5 mm/min was used for the DCB tests, as recommended by the ASTM standard D-5528-94a [20]. This standard refers to unidirectional composites, and to the authors' knowledge no equivalent standard exists for multidirectional composites. A lower displacement rate of 0.0254 mm/min was set in the notched laminates. Strain gages are added in the middle of each notched specimen, as shown in Fig. 2.

3. Delamination growth results

Crack propagation in the cross-ply specimens occurred from the delamination starter, located between the 0° and the 90° plies in the center of the beam. The crack growth was observed on both sides (sides A and B in Fig. 1). Initially, the two ends of the crack did not propagate at the same rate at the sides of the specimen. As loading increased, both crack ends seemed to propagate at the same rate. Fig. 3 shows a picture taken during one of the DCB tests. Tests were performed on unidirectional 0° specimens. In this case, crack growth was not achieved as the bond between specimen and piano hinges failed earlier. Therefore, results are not reported for this case. The cross-ply specimens studied here showed a deflection of the remote edge away from the load application, similar to the deflection shown in Fig. 3.

The crack propagation observed in the DCB experiments occurred with branching, i.e. the crack crossed the thickness of the 90° ply and then propagated parallel to the specimen axis (indicated in Fig. 1). This behavior repeated itself several times in each of the DCB tests. Crack lengths are measured as projections along the direction of the initial delamination (parallel to the specimen axis). These data are used to examine the ability of the FE model to predict crack propagation. Crack branching is not the focus of this study, instead, the overall crack propagation is used herein as the delamination measure in the DCB laminates.

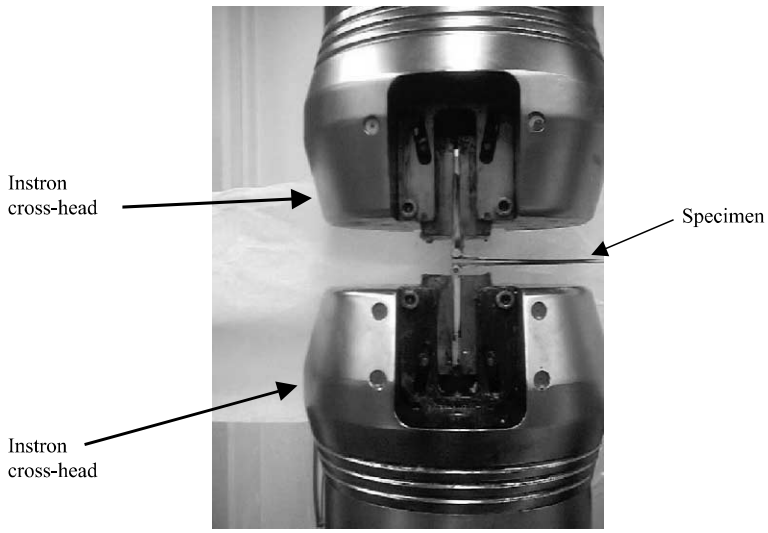

Fig. 3. Picture taken during a DCB test on a delaminated specimen.

The notched-edge laminated tension specimens are used in the study to model and examine the highly constrained crack growth in the $[90]_{20}$ laminates. The goal is to compare the FE cohesive parameters with those in the DCB model. Also, it is not clear if the cohesive parameters will capture the highly constrained crack propagation in this mode. A lower displacement rate is selected (0.0254 mm/min) to allow collecting strain data in each of the tested specimens. Measurement of crack propagation was not possible due to its dynamic nature, but the strain data allowed response verification of the FE model prior to failure.

4. Crack propagation finite element models with cohesive elements

To assess whether plane strain can be assumed, it is necessary to consider that a crack front in a DCB specimen has a parabolic distribution across the width of the specimen [15,18,21]. This is also confirmed by the non-uniform distribution of strain energy release rate across the width. Davidson and Schapery [15] introduced a parameter to quantify how uniform the distribution of strain energy release rate is. This parameter is called D_c and is defined as:

$$D_c = \frac{D_{12}^2}{D_{11}D_{22}}$$

where D_{11}, D_{12}, D_{22} are flexural rigidities (according to the conventional notation for classical plate theory). The flexural rigidities are calculated for each leg (part) of the DCB specimen. If $D_c < 0.25$ for the two legs, and each leg is orthotropic (i.e. $B_{ij} = A_{16} = A_{26} = D_{16} = D_{26} = 0$), one can consider the strain energy release rate to be approximately uniform across the width [20]. This also justifies a plane strain assumption for the FE model. The parameter D_c is calculated for the configurations used by Davidson [18], and those values are reproduced. However, the lay-ups considered herein are: $[0/0]_n$, $[\pm 15]_n$, $[\pm 45]_n$, $[\pm 60]_n$, $[\pm 75]_n$, $[90/90]_n$, $[0/90]_n$, $[0/\pm 45/90]_m$, and $[0/90/\pm 45]_m$. The TOHO UT500 graphite/epoxy material properties with an average ply thickness of 0.1275 mm were used. The quantities A_{16}, A_{26}, D_{16}, D_{26} are calculated and are equal to zero for the lay-ups with n stacking sequence. The bending–extension stiffness components, B_{ij}, are identically zero only for the cases of $[0/0]_n$ and $[90/90]_n$ (symmetric laminates). The value of D_c does not change with the number n of sub-laminates; it is sufficient to calculate D_c for the sub-laminate in those cases. However, the magnitude of the bending–extension stiffness components does change with n, and the material of the two legs approximately approaches orthotropy for large n. Table 1 reports the values of D_c for the lay-ups considered. The trend noticed in Refs. [15,18] is confirmed for the current lay-ups: D_c is maximum for $[\pm 45]_n$ lay-ups.

The DCB laminates in this study consist of $[0/90]_{10}$ lay-ups. The values of D_c for each half of the specimen, $[0/90]_5$, is 0.002444. Due to the symmetry of each half specimen, the condition of orthotropy of the two parts is verified. Therefore, the hypothesis of plane strain is acceptable, and a two-dimensional (2D) FE model can be used to study the crack propagation.

2D FE models are used in this study to simulate the delamination of the $[0/90]_{10}$ graphite/epoxy laminates. The geometric model for the delamination problem in the DCB specimens is a plate with 137 mm length, 2.55 mm thickness and 25.4 mm width. The initial crack starts at a distance of 46 mm from the edge.

Table 1
Values of the parameter D_c for the given lay-ups

Lay-up	$[0/0]_n$	$[\pm 15]_n$	$[\pm 30]_n$	$[\pm 45]_n$	$[\pm 60]_n$	$[\pm 75]_n$	$[90/90]_n$	$[0/90]_n$	$[0/\pm 45/90]_m$	$[0/90/\pm 45]_m$
D_c	9.16e−3	0.0816	0.3685	0.5190	0.3685	0.0816	9.16e−3	2.44e−3	(0.0366, $m = 10$) (0.0388, $m \gg 1$)	(0.050, $m = 10$) (0.0389, $m \gg 1$)

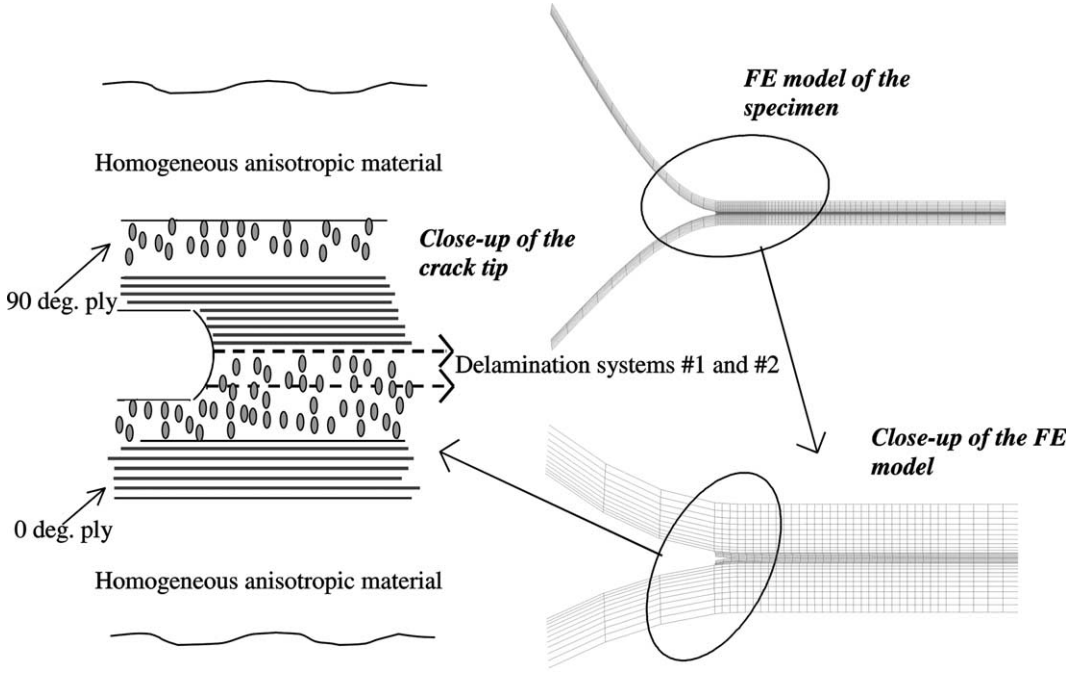

Fig. 4. Crack propagation simulation for DCB $[0/90]_{10}$ laminate.

Growth is simulated using a layer of cohesive elements and it is allowed along a 44 mm line. Two simultaneous systems of predetermined crack paths in the $[0/90]_{10}$ laminate are used, as shown in Fig. 4.

The first system allows crack growth at the interface between the 0° and 90° plies in the mid-section of the model. The second delamination system is inside the 90° ply.

The ABAQUS implicit FE code [22] is used with 4-node continuum plane strain elements (CPE4R). A convergence study of the 2D model is first carried out. The final model includes 2620 nodes and 2384 elements.

Displacement loading is applied at the top and bottom nodes of the left edge. The corresponding reaction forces are calculated for a given applied displacement. The boundary conditions applied reflect the DCB tests: the remote edge of the specimen, away from the load application, is allowed to deflect along the y-axis. This may occur due to non-symmetric application of the load through the Instron's cross-heads, and also by the non-symmetry of the laminate.

Failure of the notched laminates is modeled using a transverse cohesive layer between two notches. The geometry of the model is 135 mm in length, 25.4 mm in width and 2.62 mm thickness with notched radius of 3 mm, as shown in Fig. 2. The FE models for the $[90]_{20}$ laminate include 4-node plane-strain elements (CPE4). Finer mesh is used near the location of the crack. Half-symmetric model is applied in order to employ the traction separation failure criterion as required by the ABAQUS FE code (this is not required when using a crack tip opening displacement failure criterion). A convergence study is initially performed and a mesh with 1744 elements and 1948 nodes is used.

Uniform displacement is applied to the left edge by pulling those nodes in x-axis, as shown in Fig. 5.

A through-the-thickness homogenization procedure is employed in the DCB laminate for the remote layers away from the crack. The goal is to generate effective properties for a homogeneous continuum, that are equivalent to the multilayered medium with a repeated [0/90] sub-laminate. This allows a simplified

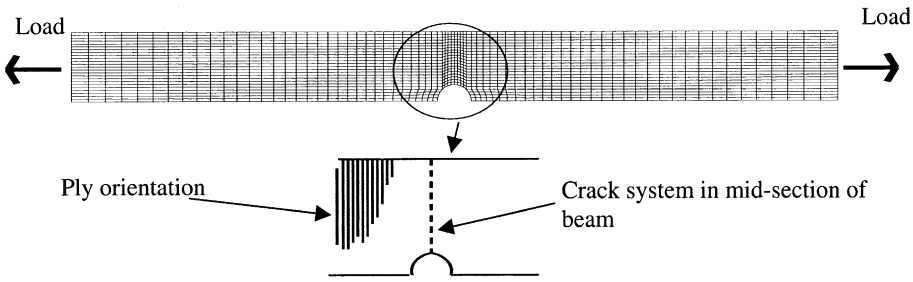

Fig. 5. FE model (half symmetry is used) for $[90]_{20}$ notched laminate.

model without several through-the-thickness elements for each lamina away from the crack. The equivalent homogenized medium and the individual 0° and 90° layers are shown in Fig. 4. Therefore, three sets of material properties are used in the FE model, where individual layers are modeled only near the interface crack. The homogenization method (Appendix A) is based on the three-dimensional (3D) lamination theory of Pagano [23]. It is generalized to non-linear behavior and applied in FE models by Haj-Ali and Pecknold [24]. The anisotropic effective properties for the $[0/90]_n$ laminate are: $E_{11} = 67.25$ GPa; $E_{22} = 67.25$ GPa; $v_{12} = 0.0494$; $G_{12} = 5.75$ GPa. This homogenization is physically acceptable because crack growth occurs within few layers of the cross-ply specimens. When non-self-similar crack growth happened, it was confined in an area of the order of one ply thickness.

5. Traction separation failure criterion and crack growth calibration parameters

Two possible crack paths are embedded in the model for the DCB cross-ply specimens. The first is at the interface between the 0° and 90° layers, at the center of the beam geometry. A second crack path is also considered within the 90° layers, as shown in Fig. 4. The two crack paths are referred to as crack system #1 and #2. A critical traction failure criterion for the crack propagation is used. The failure criterion includes normal and shear stress components, and expressed as:

$$f = \sqrt{\left(\frac{\sigma_n}{\sigma_n^f}\right)^2 + \left(\frac{\tau}{\tau^f}\right)^2} = 1 \quad \text{for failure}$$

where σ_n is normal stress component, and τ is shear stress. The cohesive layer's normal and shear failure stresses are σ_n^f and τ^f respectively. The DCB model is considered to be subject to Mode I loading, and its opening displacement criterion depends only on the normal stress component. In addition to the failure criterion parameters (σ_n^f in our case), crack growth parameters are needed. These are used to specify the manner in which the traction across the failed interface is ramped to zero. The parameters of the traction separation curve are a function of continued opening displacement or pseudo-time.

Preliminary investigation showed that the stresses do eventually merge with the singular stress field expected for a homogeneous crack roughly two elements in distance away from the notch tip. While the objective of this study is to model the propagating crack, achieving an exact singularity at the tip may not be crucial since the fracture criterion is not localized and does not directly deal with the exact order of the singularity.

The parameters used in the calibration procedure for crack growth are illustrated in Fig. 6. The distance L_c from the crack tip is where the failure criterion evaluated, and is used as the minimum length of the cohesive layer's width. The maximum time increment is assumed to be $0.5L_e$ (L_e = length of the cohesive

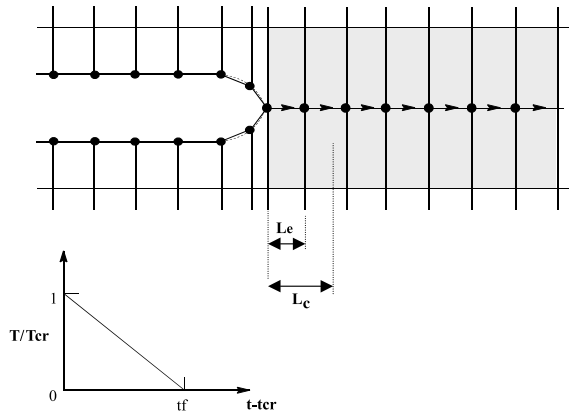

Fig. 6. Crack tip blunt area with a linear traction separation curve.

element) divided by the total applied displacement. The time to complete debonding (t_f) is chosen to be three times the allowed maximum time increment. The critical time (t_{cr}) is the time at failure initiation.

6. Case studies

Figs. 7 and 8 show the load deflection and crack growth for the DCB model with different normal stress failure values. As expected, high values of bonding stress will delay crack progression and increase the ultimate limit load.

The effect of different debonding traction separation amplitudes on the overall response has been studied. The traction is reduced to zero as a function of the time after debonding failure occurs. If the stresses are removed too rapidly, numerical convergence difficulties may arise.

The cohesive element parameters are first calibrated in the DCB problem with only one crack at the center (system #1). The experimental load deflection curve is used for this calibration, as shown in Fig. 9. The cohesive normal strength is determined as $\sigma_n^f = 27.5$ MPa, the time at which interface tractions is

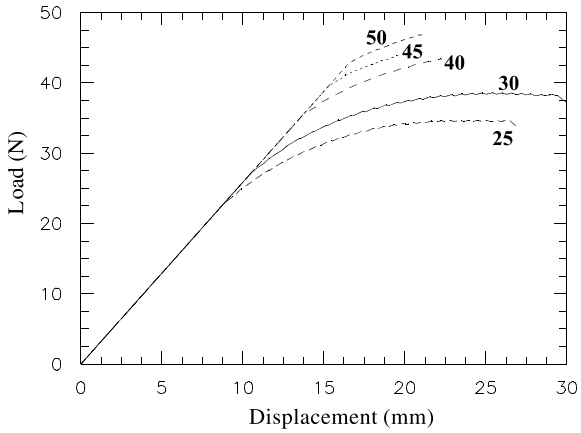

Fig. 7. Load vs. displacement from the DCB FE model with different bond normal strength values (from 25 to 50 MPa).

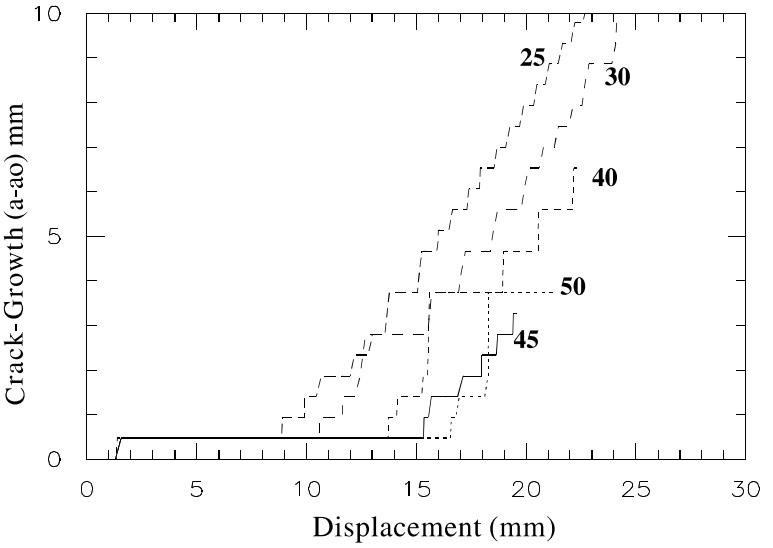

Fig. 8. Delamination crack growth vs. displacement for DCB, FE models with different bond normal strength values (from 25 to 50 MPa).

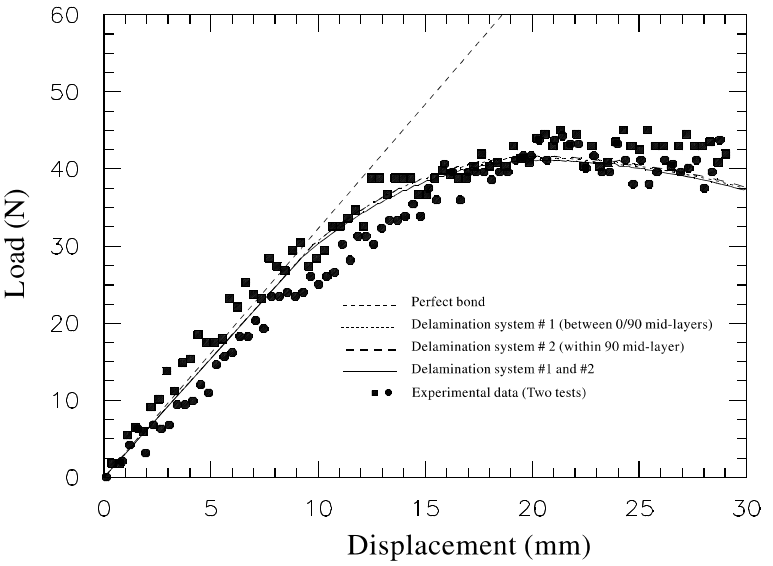

Fig. 9. Calibrated FE and experimental response for DCB model based on the load–displacement curves.

ramped to zero is $t_f = 0.01875$, and the distance from the current crack tip is $L_c = 0.25$ mm. These cohesive parameters are used in two other models, one with crack system #2 alone, and another that includes a combination of crack system #1 and #2.

The generated results from the model with two simultaneous crack systems are very close to those of the other models. In addition, the crack growth predictions for all models are in good agreement with the experimental results, as seen in Fig. 10.

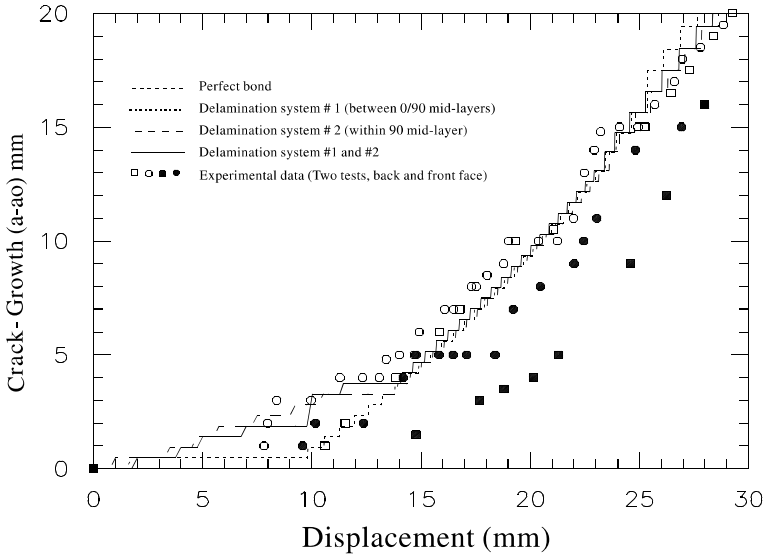

Fig. 10. Crack growth vs. displacement for the DCB specimens.

A second case study is used to simulate in-plane transverse crack growth between two notched edges. The cohesive parameters are calibrated from the experimental results of a notched $[90]_{20}$ laminate using its load–displacement curve. The cohesive normal strength is determined as $\sigma_n^f = 45$ MPa, the time at which the interface tractions go to zero is $t_f = 0.01875$, and the distance from current crack tip is $L_c = 0.25$ mm. Fig. 11 shows the ability of the proposed model to simulate the load–deflection curve and capture the rapid fracture of the notched plate.

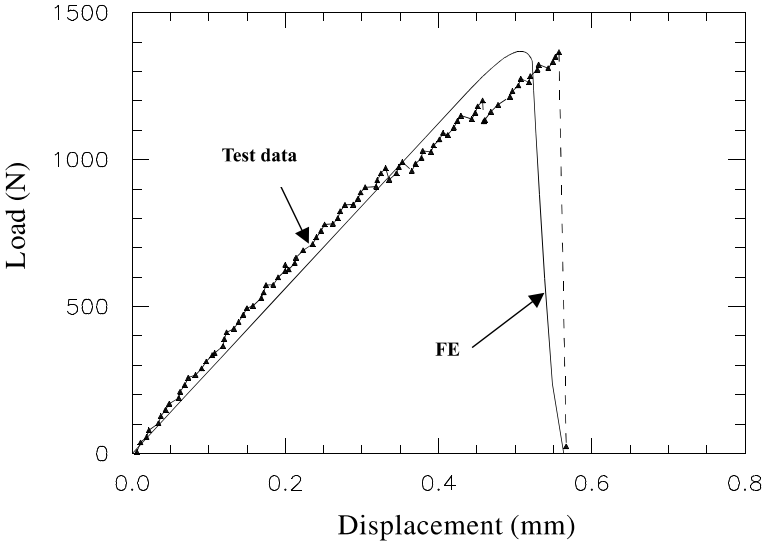

Fig. 11. Load vs. displacement from experiments and FE model, for notched-edge laminate.

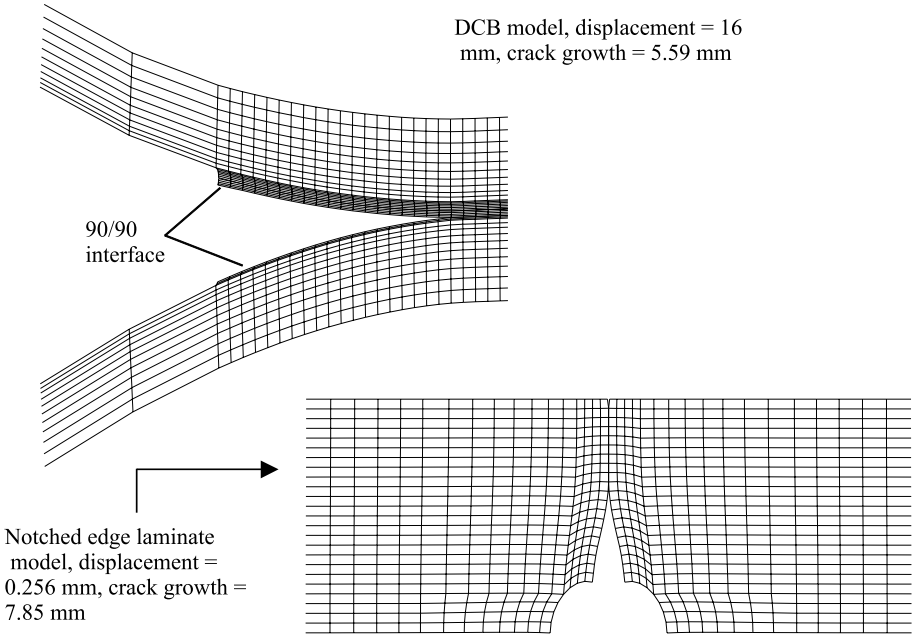

Fig. 12. Deformed shapes for the DCB and notched-edge laminate models.

The deformed shapes for the DCB FE model and the notched laminate FE model are shown in Fig. 12. The DCB FE model is shown when the crack growth is 5.59 mm, and the applied transverse displacement is 16 mm. The notched FE model is shown when the crack growth is 7.85 mm and the applied axial displacement is 0.256 mm. It is interesting to note the initiation of the crack at the center of the notched laminate, which would link afterwards with the edge crack.

7. Conclusions

A combined FE and experimental approach is presented in order to simulate the crack propagation in multilayered $[0/90]_{10}$ DCB beams and $[90]_{20}$ notched-edge laminates. The assumption of plane strain behavior in DCB models is acceptable according to a criterion based on the laminate bending stiffnesses. The study neglects mixed-mode phenomena like crack branching. The predicted FE crack propagation and strain in the notched laminate results are in good agreement with the experimental values. The proposed analysis can simplify the testing of multidirectional specimens for fracture toughness. It is shown that for multilayered DCB laminates under plane strain conditions it is sufficient to calibrate the cohesive elements from the experimental load–displacement data. The dynamic crack growth in notched laminates is also captured in the FE model.

Acknowledgements

The first author would like to acknowledge the support of Zonta International Foundation and Clare Booth Luce Foundation. The NSF support under CAREER grant number 9876080, through the Division of Civil and Mechanical Systems, to the third author is gratefully acknowledged. The fourth author would

like to acknowledge the financial support of the Office of Naval Research, Ship Structures S&T Division, grant N00014-90-J-1995, and of the Air Force Office of Scientific Research, grant F49620-98-1-0384, as well as the interest and encouragement of the grant monitors, Dr. Y.D.S. Rajapakse, Dr. Brian Sanders and Dr. Ozden Ochoa.

Appendix A

The determination of the equivalent continuum for the composite section from the equivalent properties of the layers is done using the 3D lamination theory by Pagano [23]. In this approach, the stiffness is generated for the entire section. This formulation is based on linear elasticity solutions that satisfy simple homogeneous boundary conditions, interface traction and displacement continuity between the composite layers. The properties of the equivalent homogeneous material are formulated for a repeating stacking sequence. Displacement and traction continuity conditions between the layers are satisfied and homogeneous in-plane strain and out-of-plane stress patterns are used to generate the equivalent response [24]. For the application of the 3D lamination theory, the stress–strain relationship is represented in the form

$$\begin{Bmatrix} \{\sigma_i\} \\ \{\sigma_o\} \end{Bmatrix} = \begin{bmatrix} [C_{ii}] & [C_{io}] \\ [C_{oi}] & [C_{oo}] \end{bmatrix} \begin{Bmatrix} \{\varepsilon_i\} \\ \{\varepsilon_o\} \end{Bmatrix} \tag{A.1}$$

where subscript i refers to in-plane and subscript o refers to out-of-plane stress or strain components. This system of 6 by 6 equations can be partially inverted in the following form:

$$\{\varepsilon_o\} = [C_{oo}]^{-1}\{\sigma_o\} - [C_{oo}]^{-1}[C_{oi}]\{\varepsilon_i\} \tag{A.2a}$$

$$\{\sigma_i\} = ([C_{ii}] - [C_{io}][C_{oo}]^{-1}[C_{oi}])\{\varepsilon_i\} + [C_{io}][C_{oo}]^{-1}\{\sigma_o\} \tag{A.2b}$$

$$\begin{Bmatrix} \{\sigma_i\} \\ \{\varepsilon_o\} \end{Bmatrix} = \begin{bmatrix} [A] & [B] \\ -[B]^T & [D] \end{bmatrix} \begin{Bmatrix} \{\varepsilon_i\} \\ \{\sigma_o\} \end{Bmatrix} \tag{A.3}$$

$$[A] = [C_{ii}] - [C_{io}][C_{oo}]^{-1}[C_{oi}]$$

$$[B] = [C_{io}][C_{oo}]^{-1}$$

$$[D] = [C_{oo}]^{-1}$$

The stress and strain relations used in the homogenization process are:

$$\begin{Bmatrix} \{\varepsilon_i\} \\ \{\sigma_o\} \end{Bmatrix}^{(k)} = \begin{Bmatrix} \{\varepsilon_i\} \\ \{\sigma_o\} \end{Bmatrix}$$

and

$$\begin{Bmatrix} \{\sigma_i\} \\ \{\varepsilon_o\} \end{Bmatrix} = \frac{1}{t}\sum_{k=1}^{n} t_k \begin{Bmatrix} \{\sigma_i\} \\ \{\varepsilon_o\} \end{Bmatrix}^{(k)}$$

where vectors with superscript (k) denote stress or strain for layer (k) in the global coordinate system. The overall partially inverted stress–strain relations for the entire cross-section are recovered from all layers in the sub-laminates:

$$\begin{Bmatrix} \{\sigma_i\} \\ \{\varepsilon_o\} \end{Bmatrix} = \left(\frac{1}{t}\sum_{k=1}^{n} t_k \begin{bmatrix} [A] & [B] \\ -[B]^T & [D] \end{bmatrix}^{(k)} \right) \begin{Bmatrix} \{\varepsilon_i\} \\ \{\sigma_o\} \end{Bmatrix} \tag{A.4}$$

where n is the number of layers in the sub-laminate. Writing the above relation in a similar form as Eq. (A.3) yields:

$$\begin{Bmatrix} \{\sigma_i\} \\ \{\varepsilon_o\} \end{Bmatrix} = \begin{bmatrix} [A] & [B] \\ -[B]^T & [D] \end{bmatrix} \begin{Bmatrix} \{\varepsilon_i\} \\ \{\sigma_o\} \end{Bmatrix} \tag{A.5}$$

The well-known overall stiffness relation for the section is:

$$\begin{Bmatrix} \{\sigma_i\} \\ \{\sigma_o\} \end{Bmatrix} = \begin{bmatrix} [C_{ii}] & [C_{io}] \\ -[C_{oi}]^T & [C_{oo}] \end{bmatrix} \begin{Bmatrix} \{\varepsilon_i\} \\ \{\varepsilon_o\} \end{Bmatrix} \tag{A.6}$$

Finally Eq. (A.6) can be inverted to generate the engineering coefficients for the homogenized equivalent medium.

References

[1] Comninou M. An overview of interface cracks. Eng Fract Mech 1990;37(1):197–208.
[2] Suo Z. Singularities, interfaces and cracks in dissimilar anisotropic media. Proc R Soc London A 1990;427:331–58.
[3] Williams ML. The stress around a fault or crack in dissimilar media. Bull Seismol Soc Am 1959;49:199–204.
[4] England H. A Crack between dissimilar media. J Appl Mech 1965;32:400–2.
[5] Erdogan F. Stress distribution in bonded dissimilar materials with cracks. J Appl Mech 1965;32:403–10.
[6] Comninou M. The interface crack. J Appl Mech 1977;44:631–6.
[7] Comninou M. The interface crack in a shear field. J Appl Mech 1978;45:287–90.
[8] Gautesen AK, Dundurs J. The interface crack in a tension field. J Appl Mech 1987;54:93–8.
[9] Gautesen AK, Dundurs J. The interface crack under combined loading. J Appl Mech 1988;55:508–86.
[10] He M-Y, Hutchinson JW. Kinking out of a crack out of an interface. J Appl Mech 1989;56:270–8.
[11] Qu J, Bassani J-L. Cracks on bimaterial and bicrystal interfaces. J Mech Phys Solids 1989;37(4):417–34.
[12] van der Zande HD, Grootenboer HJ. A finite element approach to interface cracks. J Appl Mech 1986;53:573–8.
[13] Hwu C, Kao CJ, Chiang LE. Delamination fracture criteria for composite laminates. J Compos Mater 1995;29(15):1962–87.
[14] Dakshina Moorthy CM, Reddy JN. Recovery of interlaminar stresses and strain energy release rates in composite laminates. Finite Elem Anal Des 1999;33(1):1–27.
[15] Davidson BD, Schapery RA. Effect of finite width on deflection and energy release rate of an orthotropic double cantilever specimen. J Compos Mater 1988;22:640–56.
[16] Davidson BD, Hu H, Schapery RA. An analytical crack-tip element for layered elastic structures. J Appl Mech 1995;62:243–53.
[17] Davidson BD, Yu L, Hu H. Determination of energy release rate and mode mix in three-dimensional layered structures using plate theory. Int J Fract 2000;105:81–104.
[18] Davidson BD. An analytical investigation of delamination front curvature in double cantilever beam specimens. J Compos Mater 1990;24:1124–37.
[19] Polaha JJ, Davidson BD, Hudson RC, Pieracci A. Effect of mode ratio, ply orientation and precracking on the delaminated toughness of a laminated Composite. J Reinf Plast Compos 1996;15:141–72.
[20] Standard test method for Mode I interlaminar fracture toughness of unidirectional fiber-reinforced polymer matrix composites, 1994. ASTM D-5528-94a.
[21] Crews JH, Shivakumar KN, Raju IS. Strain energy release rate distributions for double cantilever beam specimens. AIAA J 1991;29(30):1686–91.
[22] ABAQUS, Hibbitt, Karlsson and Sorensen Inc., User's Manual, Version 5.8, 1998.
[23] Pagano NJ. Exact moduli of anisotropic laminates. In: Sendeckyj GP, editor. Mechanics of composite materials. New York: Academic Press; 1974. p. 23–44.
[24] Haj-Ali RM, Pecknold DA. Hierarchical material models with microstructure for nonlinear analysis of progressive damage in laminated composite structures. Structural Research Series No. 611, UILU-ENG-96-2007, 1996, Department of Civil Engineering, University of Illinois at Urbana-Champaign.